42nd AIAA Fluid Dynamics Conference and Exhibit
25 - 28 June 2012, New Orleans, Louisiana

AIAA 2012-3075

On the stability of flows over rough rotating disks

Joseph H. Harris* and Peter J. Thomas†
University of Warwick, Coventry, Warwickshire, CV4 7AL, United Kingdom
Stephen J. Garrett‡
University of Leicester, Leicester, Leicestershire, LE1 7RH, United Kingdom

We consider the effects of distributed roughness on the boundary-layer transition over a rotating disk using both theoretical and experimental approaches. The theoretical approach further develops Yoon *et al.*'s method [*Int. J. Heat Fluid Flow*, 28, p262 (2007)] for obtaining the steady-flow solutions for a general surface distribution function. Full three-dimentional stability analyses are conducted on these for a range of roughness parameters. The experimental approach seeks to verify the steady-flow solutions and investigate the transition mechanisms at play with increasing surface roughness. Both approaches yield consistent results that suggest that surface roughness could lead to a transition mechanism that bypasses the usual cross-flow mechanism.

Nomenclature

λ	Boundary layer thickness
δ	Roughness height
γ	Roughness wavelength
s	Surface function
α	Radial wavenumber
β	Azimuthal wavenumber
ω	Disturbance frequency
n	Number of vortices
R_{crit}	Critical instability Reynolds number
Ω	Disk rotating rate
ν	Kinematic viscosity
ζ	Transformed z-coordinate

I. Introduction

It is now firmly established that the classic belief that surface roughness inevitably increases skin-friction drag no longer holds.[1–5] The *right sort of roughness* can reduce drag due to energetically beneficial interactions between coherent, energy-bearing eddy structures and roughness protrusions within the boundary layer. A challenge for the next few decades remains to identify what constitutes the *right sort of roughness* for any given particular type of boundary layer and for the intended specific technological application. With this motivation in mind, we study the effects of roughness on a generic type of boundary-layer flow that is of major relevance to numerous practical applications: the rotating disk.

For practical and theoretical reasons the flow created over a rotating disk has served as the paradigm for studying boundary layers with cross-flow component for over six decades.[6–12] However, despite its relevance to many practical applications (for instance, on highly swept wings or on many types of rotating machinery),

*PhD Student, Fluid Dynamics Research Centre, University of Warwick.
†Professor, Fluid Dynamics Research Centre, University of Warwick.
‡Senior Lecturer, Department of Mathematics, University of Leicester.

it is recognized that previous work on the 3D rotating-disk flow is mostly limited to flow transition over smooth disks only.[13] For instance, experimental studies have focused almost exclusively on disks designed to test theoretical predictions obtained for hypothetical, idealized flow conditions. These are rarely present in real-world engineering environments.

It is emphasized that we study the effects of realistic, uniform distributed roughness of increasing levels and different types, and not the effects of a small number of roughness elements as, for instance, in Ref. 14–18.

The beginning of the natural transition process of the boundary layer over rotating disks and other rotating bodies (e.g. a cone or sphere) is signaled by the development of the well-known stationary spiral vortices within the transition region.[8–12, 17–23] Ref. 13 reports the very interesting result that a modest roughness level of approximately 19μm decreased the number of these vortices from initially 32 for a smooth disk to 26 for the rough disk. This raises questions as to whether roughness levels above 19μm can reduce the number of spiral vortices further and whether transition can possibly bypass the spiral-vortex route entirely above a certain critical roughness level. This would indicate roughness promoting an entirely different transition mechanism and warrants further study since it will be associated with different energetical implications.

There appears to exist only two previous studies[24,25] that tackled the important question of how successively increasing roughness levels affect the radial and azimuthal components of the steady-flow velocity within the boundary layer and, therefore, how roughness leads to deviations from the classic von Kármán similarity solution[26] for these profiles. However, the computational results of Ref. 24, 25 have not been corroborated in experiments.

Our main goal is to investigate how successively increasing levels of distributed surface roughness and different roughness types affect transition and the overall flow of the generic fully 3D rotating-disk boundary layer. The approach is split into two distinct, but closely interconnected, parts of experimental and theoretical research. The main goal of this preliminary investigation is to clarify the modifications to the well-known stability characteristics of smooth disks with increasing levels of roughness; following this the possibility of a potential bypass transition will be studied.

II. Theoretical approach

II.A. The steady flow profiles

We follow the approach of Yoon *et al.*[25] to model the surface roughness, however some modifications to their approach have been made. The surface of the disk is described by $s^* = a^* \cos(2\pi r^*/\gamma^*)$, with * indicating a dimensional quantity. The quantity a^* is the amplitude of the surface variation from its mean value, γ^* is the wavelength of the surface variation, and r^* is the distance along the disk in the radial direction. The surface function can be altered to suit any required profile by changing the value of a^* and γ^*, along with the functional form (we use the cos function throughout this study). The disk is considered to be rotating about its axis of symmetry at a rotation rate Ω^*. It is natural to consider this geometry in a fixed cylindrical polar coordinate system (r^*, θ, z^*) in which the governing Navier–Stokes equations are well known. The steady-flow components in these directions are denoted (u^*, v^*, w^*).

All dimensional quantities are scaled on a characteristic length-scale given by the boundary-layer thickness, $\lambda^* = \sqrt{\nu^*/\Omega^*}$, and the velocity scale given by $\lambda^*\Omega^*$. This leads to the Reynolds number $Re = \Omega^*\lambda^{*2}/\nu^*$ which is interpreted as a measure of the spin rate. The surface function nondimensionalizes to

$$s = \delta \cos\left(\frac{2\pi r}{\gamma}\right), \tag{1}$$

with amplitude and wavelength parameters δ and γ, respectively. These are our control parameters and are expressed in units of boundary-layer thickness as a consequence of the scalings.

Before attempting to solve the governing equations, it is necessary to transform out the surface distribution. To this end we use a new coordinate system (r, θ, η) defined by the transformation $\eta = z - s(r)$. In this modified coordinate system the flow components are transformed to be

$$U = u, \quad V = v, \quad W = -s'u + w, \tag{2}$$

where the prime denotes differentiation with respect to r. At this stage we make the boundary-layer assumption, $Re^{-1} << 1$, and set $\zeta = Re^{1/2}\eta$, $\tilde{W} = Re^{1/2}W$.

The governing equations for the steady flow are obtained after introducing variables closely related to the von Kármán similarity variables,

and are stated as

$$2f + r\frac{\partial f}{\partial r} + \frac{\partial h}{\partial \zeta} = 0, \tag{3}$$

$$rf\frac{\partial f}{\partial r} + h\frac{\partial f}{\partial \zeta} + f^2\left(1 + r\frac{s's''}{1+s'^2}\right) = (1+s'^2)\frac{\partial^2 f}{\partial \zeta^2} + \frac{g^2}{1+s'^2}, \tag{4}$$

$$rf\frac{\partial g}{\partial r} + h\frac{\partial g}{\partial \zeta} + fg = (1+s'^2)\frac{\partial^2 g}{\partial \zeta^2} - fg. \tag{5}$$

These are subject to the boundary conditions

$$\begin{aligned} f(r) = h(r) = 0, \;\; g(r) = 1 \quad & \text{at } \zeta = 0, \\ f(r) = g(r) = 0 \quad & \text{as } \zeta \to \infty, \end{aligned} \tag{6}$$

which represent the no slip and quiescent fluid conditions at all radial positions in this frame of reference. Note that this system reduces to the von Kármán system of ODEs in ζ when $s(r) \to 0$, as would be expected.

Equations (3)–(6) can be solved to find the velocity profiles for a disk with a surface distribution parameterized by δ and γ using the commercially available NAG routine D03PEF. The routine is a PDE solver, which reduces the PDEs to a system of ODEs in ζ using the method of lines. The ODEs are then solved using the backwards difference method. The solver uses an initial solution at $r = 0$ to find the values for the velocity profiles at the next increment of r and marches forward. The velocity profiles at each r are found using a grid between $\zeta = 0$ and 15. The initial solution at $r = 0$ is found using a series-solution method first described by Banks[27] and more recently used by Garrett & Peake[20] in a similar context. Within this approach the functions f, g and h are expanded using a series expansion in terms of increasing powers of r, and these expansions are substituted into Eq. (3)–(6). Since we require the solution at $r = 0$, we can ignore all higher order terms and consider the resulting ODE system in ζ at leading order. This leaves us with the familiar set of von Kármán equations, demonstrating that the leading-order solution for the rough disk is that of the smooth disk, irrespective of the function used to describe the surface.

The theoretical flow profiles resulting from the NAG solution are dependent on the radial position r, owing to the introduction of $s(r)$. However, the cyclical nature of $s(r)$ means that the flow profiles have a cyclical nature themselves, characterized by the wavelength parameter γ. This is in contrast to the usual von Kármán solution, where all position dependence is contained within the similarity transformation. However, given the small wavelengths involved in these distributions ($\gamma^* = O(\lambda^*)$), it is possible to revert back to a von Kármán type flow for the purposes of the stability analysis by using a single profile obtained from the ensemble-averaged flow from 100 flows at evenly spaced locations over one wavelength. This has the significant advantage that, in this preliminary study at least, previous stability codes developed for the smooth disk[21,22] can be used enabling a direct comparison between the results over smooth and rough disks.

Figure 1 shows the results from ensemble averages of flows over one wavelength from $r = 3$ (although the solution is independent of this location). For the purpose of comparing variations of the parameters γ and δ, the ratio δ/γ will be used for simplicity. The results are shown from $\delta/\gamma = 0$ to $\delta/\gamma = 0.2$ as roughness is increased from the smooth case. For the radial flow (f-velocity profile), roughness is seen to decrease the maximum fluid velocity within the boundary layer, i.e. roughness acts to reduce the wall jet. This is physically sensible as roughness would increase the friction holding the base of the wall jet back as it moves along the radius of the disk. For the azimuthal case (g-velocity profile), roughness is seen to broaden the boundary layer through a thickening of this profile; again, this is physically sensible. The normal flow (h-velocity profile) is seen to increase the flow entrained into the boundary layer. However, the use of the boundary-layer assumption means that this component is actually an order of magnitude smaller than the other components and has only minor implications for the stability of the flow.

II.B. Stability analysis

Now that the steady flows for the rough disks have been obtained, the next stage in the theoretical study is to perform stability analysis for a range of values of parameters δ and γ.

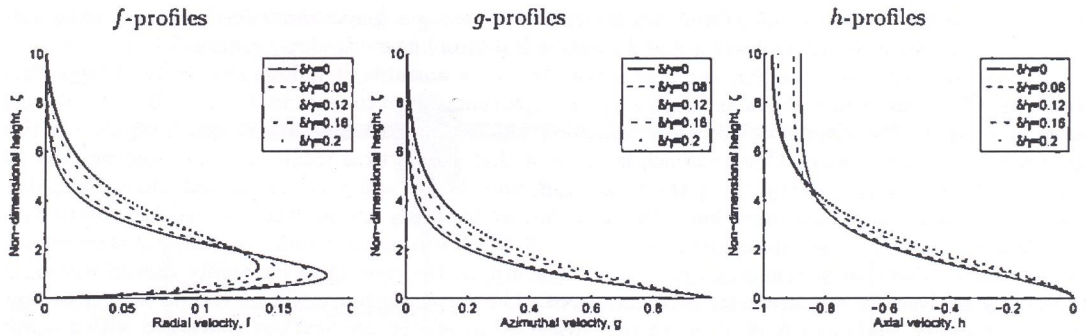

Figure 1: Transformed steady-flow profiles for $\delta/\gamma = 0$ to 0.2.

To do this, we consider small perturbing quantities added to the averaged steady profiles and substitute these into the governing boundary-layer equations. The perturbations are assumed to have normal mode form

$$(\bar{u}, \bar{v}, \bar{w}, \bar{p}) = (\hat{u}, \hat{v}, \hat{w}, \hat{p})(\zeta) e^{i(\alpha r + \beta Re\theta - \omega t)},$$

where α is the radial wavenumber, β is the azimuthal wavenumber, and ω the frequency. In what follows, we conduct a spatial analysis and so assume α is complex with the imaginary part giving the spatial growth rate of disturbances. Both β and ω are assumed to be real and, in order to ensure periodicity round the disk, $n = \beta Re$ (identified as the number of vortices) must be interpreted at real integer values only. Some manipulation leads to the six first-order ordinary differential perturbation equations. See Ref. 20 for more information regarding the formulation of these equations.

$$\phi_1' = \phi_2 \tag{7}$$

$$\left[\frac{\phi_2'}{R}\right] = \phi_3 \left(\left(\bar{\alpha} - \frac{i}{R}\right) U' + \bar{\beta} V'\right) i\phi_4 + \left(\bar{\alpha}^2 + \bar{\beta}^2 - \frac{i\bar{\alpha}}{R}\right) + \left[\frac{W\phi_2}{R}\right] - \left[\frac{2V\phi_5}{R}\right] + \frac{1}{R}\left(\left(\bar{\alpha}^2 + \bar{\beta}^2\right) + iR\left(\bar{\alpha}U + \bar{\beta}V - \omega\right) + U\right)\phi_1 \tag{8}$$

$$\phi_3' = -i\phi_1 - \left[\frac{\phi_3}{R}\right] \tag{9}$$

$$\left[\frac{\phi_4'}{R}\right] = -\frac{1}{R}\left(\left(\bar{\alpha}^2 + \bar{\beta}^2\right) + iR\left(\bar{\alpha}U + \bar{\beta}V - \omega\right) + W'\right)\frac{\phi_3}{R} + \left[\frac{iW\phi_1}{R}\right] - \left[\frac{i\phi_2}{R}\right] \tag{10}$$

$$\phi_5' = \phi_6 \tag{11}$$

$$\left[\frac{\phi_6'}{R}\right] = \left[\frac{2V\phi_1}{R}\right] + \left(\left(\bar{\alpha} - \frac{i}{R}\right) V' - \bar{\beta} U'\right)\phi_3 + \frac{1}{R}\left(\left(\bar{\alpha}^2 + \bar{\beta}^2\right) + iR\left(\bar{\alpha}U + \bar{\beta}V - \omega\right) + U\right)\phi_5 + \left[\frac{\bar{\beta}\phi_4}{R}\right] + \left[\frac{W\phi_6}{R}\right] \tag{12}$$

Here the prime indicates differentiation with respect to ζ and ϕ_{1-6} are dependent transformed variables taken from 20. The steady flow components U, V, and W are obtained by reversing the transformations of Eq. 2.

We solve the eigenvalue problem defined by the perturbation Eqs (7)–(12) with the homogeneous boundary conditions

$$\begin{aligned} \hat{w} &= 0, \quad \zeta = 0, \\ \hat{w} &\to 0, \quad \zeta \to \infty, \end{aligned} \tag{13}$$

which ensure that the disturbances are contained within the bounday layer. The eigenvalue problem is solved for certain combinations of values of α, β and ω at each parameter set (Re, δ, γ). From these we form the dispersion relation, $D(\alpha, \beta, \omega; Re, \delta, \gamma) = 0$, with the aim of studying the occurrence of convective

instabilities. In each analysis the α-branches are calculated using a fourth-order Runge–Kutta integrator with Gram–Schmidt orthonormalization and a Newton–Raphson linear search procedure.

Since we are supposing here that the flow is not absolutely unstable, it follows that in the Briggs–Bers procedure[20,28] we can reduce the imaginary part of the frequency down to zero, so that $\omega_i = 0$, as mentioned above. To produce the neutral curves for convective instability a number of approaches can be taken in this stationary frame of reference. One approach is to insist that the vortices rotate at some fixed multiple of the disk surface velocity, thereby fixing the ratio ω_r/β, and then α and β are calculated using the spatial analysis. This is the approach taken here. In particular, we explicitly assume that the vortices rotate with the surface of the disk (i.e. are *stationary*) so that $\omega_r = \beta$, which is consistent with experimental observations discussed in §I. Two spatial branches were found to determine the convective instability characteristics in the stability analysis for all parameter sets considered. The first branch arises from the inviscid cross flow (type I) instability mode and is identical to that discussed in related publications concerned with smooth bodies.[20,28,29] It is known that this mode arises from the inflectional nature of the streamwise mean velocity component U. Previous investigations of related boundary layers have also noted the appearance of a viscous streamline curvature (type II) instability mode. This second branch corresponds to a centrifugal instability associated with the way in which the outer-flow streamlines are curved by an $O(R^{-1})$ amount close to the outer edge of the boundary layer.

Figure 2 demonstrates the results of this preliminary stability analysis for values of δ/γ up to 0.2. It can be seen that the increase in roughness generally has a stablilizing effect on the instability mechanism, characterized by the clear narrowing of the stability curve, resulting in a decrease of the total instability region. An increase in the roughness parameters also appears to switch the dominant instability mechanism from the cross-flow (upper lobe) to the streamline curvature (lower lobe), as the former shrinks, while the latter grows. This shift in the instability mechanism also causes an increase in the critical Reynolds number as the upper lobe decreases in size. However, the critical Reynolds number falls again as the streamline curvature instability becomes the dominant mode. Furthermore, we see a lowering of the predicted number of vortices (associated with the disturbance wavenumber in the azimuthal direction). These preliminary results are consistent with Watanabe *et al.*'s[13] observation that the number of vortices reduces with roughness height, and we will seek to corroborate these findings ourselves with experiments in §III.

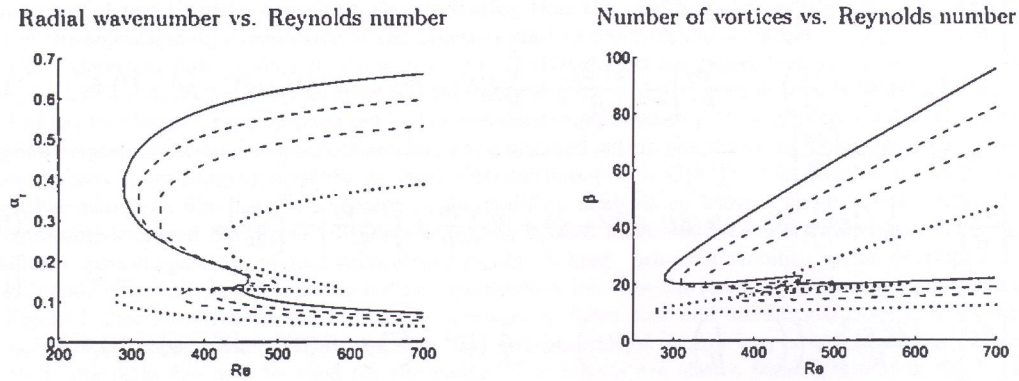

Figure 2: Neutral curves from the stability analysis of the resulting flow profiles; von Kármán (-); $\delta/\gamma = 0.08$ (- -); $\delta/\gamma = 0.12$ (-.); $\delta/\gamma = 0.16$ (···); $\delta/\gamma = 0.2$ (o).

III. Experimental approach

The experimental rig and measurement techniques used in this research already exist at Warwick, and have previously been used successfully for research into the effects of compliance on transition over rotating disks.[17,18] Our facility essentially consists of a water-filled tank (diameter 1m) housing the computer-controlled disk (diameter 0.4m), as shown in figure 3. The main measurements are carried out with a TSI IFA300 constant-temperature hot-film anemometry system. The hot-film probe on its support traverse is fully computer controlled and can be calibrated in situ. The traverse moves both horizontally and vertically,

which enables the hot-film probe to be positioned at any height and radius along the disk surface where it can take mean and fluctuating velocity readings as well as turbulence intensity measurements.

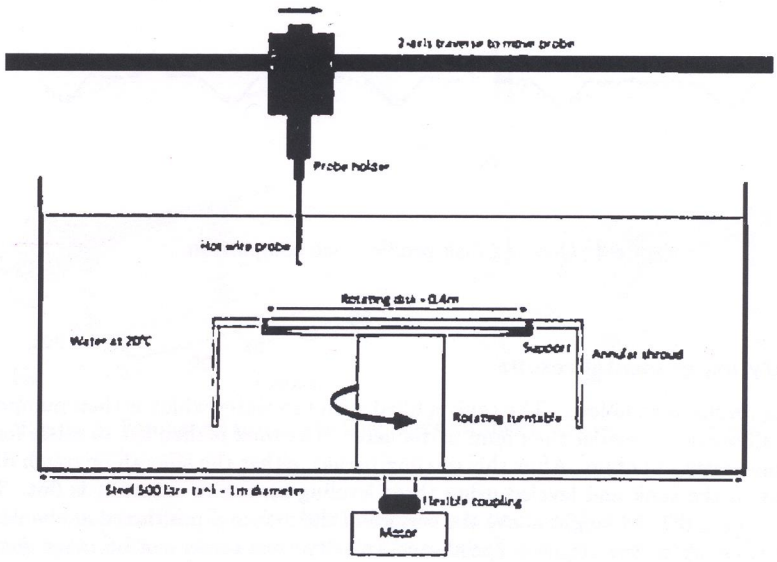

Figure 3: Diagram of the rotating-disk facility.

In order to characterize the roughness of the disks we have so far employed the classic classification scheme of *hydraulically smooth*, *transitional* or *completely rough* used, for instance, for flat-plate boundary layers or for the flow inside tubes with rough walls. However, considering the general background[19] that led to this scheme and, in particular, the fact that it was developed for fully turbulent flow, it is by no means clear in how far it will directly translate to the (transitional) rotating-disk flow. This classic roughness-classification scheme relies on the roughness parameter, $\Theta = k_s \nu^* / \nu$, where k_s is typical roughness height, $\nu^* = \sqrt{\tau_0/\rho}$ is the friction velocity, and τ_0 the wall shear stress. The larger its value the more pronounced the expected influences of roughness. Walls are classified as hydraulically smooth for $\Theta < 5$ and as completely rough for $\Theta > 70$. Roughness effects appear within the transitional regime $5 \leq \Theta \leq 70$. For typical operating conditions of our rotating-disk facility we estimate that we will need roughness protrusions within, roughly, 36μm and 500μm to cover the transitional regime - provided the classic roughness scheme for 2D flows does indeed extend to the 3D rotating disk flow. If our continuing research reveals that the classic roughness-classification scheme is not suited for fully 3D flows with cross-flow component then we will attempt to adapt the scheme for this particular type of flow.

In order to comply with the roughness classification scheme and the theoretical disk surface profile, a rough disk surface had to be found which would satisfy both these conditions. An aluminium disk was manufactured by cutting concentric grooves into the surface on a lathe, producing an approximate sinusoidal profile in the radial direction similar to the theory. The grooves can be cut at a variable depth and pitch, thus enabling us to vary the roughness height and wavelength. The disks were manufactured to have roughness heights of between 100μm and 500μm which fit within our transitional regime. To confirm the surface roughness, the disk was measured with our Rank–Taylor–Hobson Talysurf facility (see[17,18]). A stylus is dragged across the surface of the disk in a radial direction, producing a trace of the surface height. The Talysurf facility produced a profile trace which we were then able to compare to a cos wave function, see figure 4. The roughness profile of the grooved disk compares favourably with the surface function used in Eq. (1) . In addition to this rough disk, a comparitively smooth glass disk will be used to obtain smooth case results. The glass disk has a Talysurf roughness height measurement of 9.6μm, which puts it in the hydraulically smooth regime as set out above.

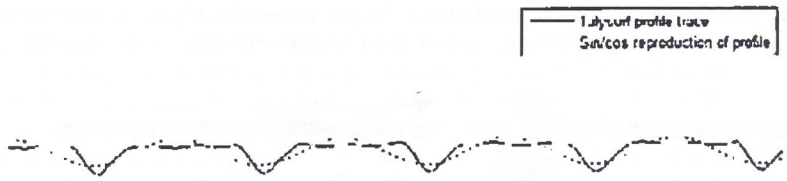

Figure 4: Grooved disk profile trace comparison.

III.A. Preliminary experimental results

The process of taking results is as follows. The tank is filled with tap water which is then pumped through a filter which removes all particles smaller than 5μm in diameter. The tank is then left to settle for 2 to 3 days to rid the water of any oxygen bubbles. After this settling period, either the smooth or rough disk is placed onto the support disk in the tank and leveled using three leveling screws to ensure it is flat. The hot-film probe is then lowered to the desired height above the surface of the disk and positioned at the desired radius.

The disk is then spun up to the required speed, and velocity time series can be taken for that radius and height. In order to remove any unwanted fluctuations, or irregularities from our data, we can take an ensemble average of multiple time series taken at the same position. When the anemometer software acquires the data, it relies on a trigger mechanism to start recording. The trigger it uses is an optical sensor situated on the rotating shaft of the main motor which turns the disk. Since it is triggered at the same point for each rotation of the disk, and it is set to record for the same length of time for each trigger, each time series can be assumed to be in sync with another and can be ensemble averaged to give one single average time series with any non-periodic fluctuations averaged out. Each time series acquires data for 1.024 seconds during which it obtains 1024 readings.

From then on, there are two approaches we can take. One approach is to keep the radial position constant (which amounts to keeping Re constant), and vary the height at which the mean velocity measurements are taken in the boundary layer in order to build up a velocity profile at that Reynolds number. By altering the direction of the probe, we can measure either the radial or azimuthal velocity profiles as shown in transformed form in figure 1 and compare with the theory. Data for this experiment is currently unavailable, but planned for the future.

For this paper however a second approach was used. The probe height was kept constant in the boundary layer, and the radius was varied, in order to build up a visialisation of how the flow changes as we move radially outwards, to highlight when it becomes turbulent, as well as looking at the stability of the flow. The approach taken is similar to Colley *et al.*[17] The non-dimensional probe height chosen for all readings was $\zeta = 1.24$, while the readings were taken at 5mm intervals along the radius. For each disk, 20 separate time series were taken at each radius, and at 30 increasing radii. Frequency spectra were created from each of the 20 velocity files at each radius by taking a fast Fourier transform of the data, before an ensemble average of each set of 20 files was taken. Figure 5 shows the averaged frquency spectra for the smooth and rough disks. The y-axis in both cases shows the square of the amplitude of the frequencies, A^2 which is proportional to the amount of energy contained within each frequency. These plots highlight the frequencies of any stationary periodic fluctuations in the flow, as well as the relative strengths of each frequency as the Reynolds number is increased. For both plots, at low Re, there are few frequencies that dominate the flow. Instead there are low levels of all frequencies from which we can deduce that the flow here is laminar and contains few fluctuations. At the highest Re, there are high amplitude frequency spectra, at a broader range of frequencies, indicating that the flow has become turbulent here near the edge of the disk.

As Re increases from the centre of the disk, there is an increase in the power spectra for both disk cases at approximately $Re = 380$ for the rough disk, and $Re = 410$ for the smooth. This point indicates where the flow has become unstable. The frequency at which this peak occurs is the frequency of the disturbance in the azimuthal direction, or the number of vortices. It is easier to ascertain the exact number of vortices

Smooth disk $\delta/\gamma = 0$ Rough disk $\delta/\gamma = 0.1$

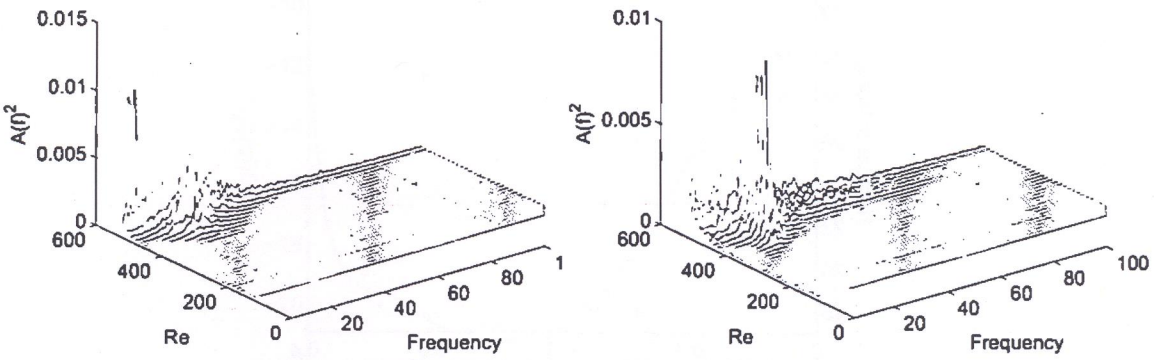

Figure 5: Frequency amplitude flow fields for disks rotating at 7.85 $rads^{-1}$

by looking at the contour plots in figure 6. From these it can be seen that the number of spiral vortices on the smooth disk is around 30, while the number on the rough disk is lower, at around 26.

Smooth disk $\delta/\gamma = 0$ Rough disk $\delta/\gamma = 0.1$

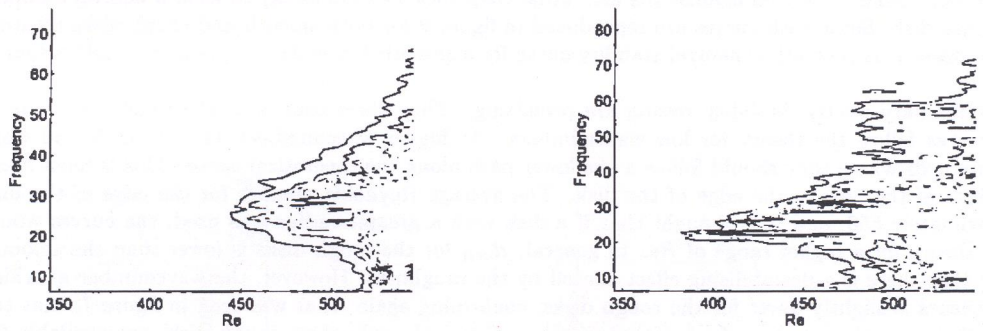

Figure 6: Contour plots indicating the number of azimuthal vortices

Frequency plots were produced for a few different rough disks rotating at various speeds, and the number of vortices observed in each case are presented in figure 7. The roughness depth for each disk has been non-dimensionalised by the boundary layer thickness, λ^* in order to compare the disks rotating at different speeds. The smooth glass disk therefore appears on the left of the plot with a relatively small roughness compared to the rough disks. There is a definite shift downwards in the number of vortices as the roughness increases, although this effect may possibly break down as the non-dimensional roughness increases beyond 0.2. More tests on a greater sample of disks planned for the future will seek to confirm this.

In order to confirm the findings from §II.B, the curve of neutral stability needs to be gained from the data. This can be done by looking at the energy, A^2 contained in the velocity signal in the frequency domain. If the energy from the frequency flow fields are extracted for individual values of the frequency and plotted on a log scale, a plot of the energy contained in the flow as one moves outwards along the radius of the disk is obtained (figure 8). This is essentially a cut taken along the Re axis from figure 5 at a specific frequency. As Re increases from the centre of the disk, the flow experiences a fall in the amount of energy. In this region any disturbance will be damped and hence the flow is stable. Towards the edge of the disk (high Re), the energy increases with the flow direction, and therefore any perturbations will be amplified. It can therefore be concluded that the turning point on the energy curve is a point of neutral stability, otherwise known as the threshold of growth. This neutral stability point can be read off the graph once a line of best fit has been

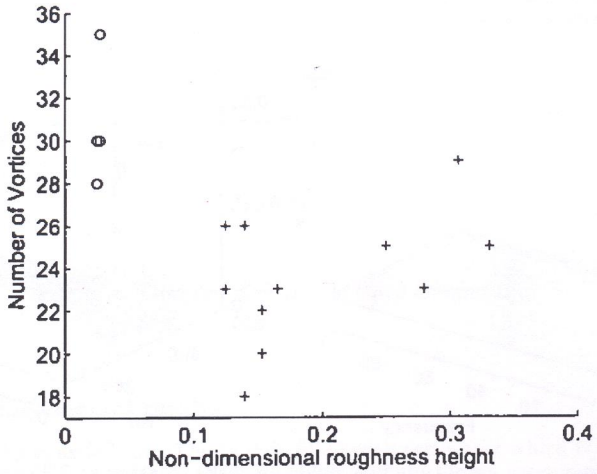

Figure 7: Observed number of spiral vortices against non-dimensional roughness height for smooth disk (o) and rough disks (+)

added to ascertain the minimum. The Reynolds number location of this growth threshold is found for many different frequencies and plotted against the azimuthal frequency (wavenumber) to form a neutral stability curve for that disk. Some such curves are reproduced in figure 9 for both smooth and rough disks rotating at different speeds. A theoretical neutral stability curve for a smooth $\delta/\gamma = 0$ case is added to help visualise the curve.

The preliminary neutral stability results are promising. They show that both the rough and smooth stability curves follow the theory for low wavenumbers. At higher wavenumbers, the curves for all disks continue upwards where they should follow a shallower path along the theoretical curve. This is most likely due to effects of the flow at the edge of the disk. The average Reynolds number for the edge of the disk was approximately 550, and it is thought that if a disk with a greater radius was used, the curves would follow the theory for a higher range of Re. In general, R_{crit} for the rough disks is lower than the smooth, suggesting that there is a destabilising effect caused by the roughness. However, the wavenumber at which the R_{crit} occurs is slightly lower for the rough disks, confirming again what was seen in figure 7, that the roughness decreases the number of azimuthal vortices. Currently only three rough disks are available for testing, and two of these disks have the same roughness ratio, δ/γ, albeit with different roughness heights. Therefore not enough results are available to ascertain the changes in the neutral curve as the roughness ratio changes. These results will be presented in the future however, after more disks are manufactured.

IV. Conclusion

A suitable theoretical model for predicting the effect of distributed roughness on the stability of the flow over a rotating disk was sought. The flat surface of the disk geometry is replaced with a surface function that can be used to mimic roughness, and this geometry is used to produce steady boundary layer flow profiles and subsequently stability curves. The model predicts a decrease in the number of azimuthal spiral vortices as well as a shift in the dominant mode of instability mechanism; from cross-flow to streamline curvature, as the roughness is increased. A slight increase in the critical Reynolds number for a small increase in roughness is followed by a decrease in R_{crit} as the roughness grows further, due to the switch in the dominant instability mode.

Grooved rough disks were manufactured to match the theoretical model in an attempt to confirm the results from the numerical study. Preliminary experimental results seem to confirm that the number of vortices will decrease for flow over a rough disk. However, we are unable to confirm a linear relationship between roughness height and decreasing vortices until more results are obtained for a greater variety of

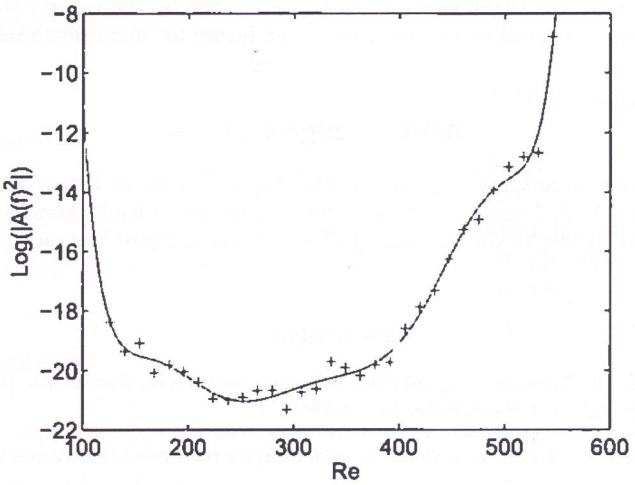

Figure 8: Energy contained within the flow for an example frequency of 20 hz.

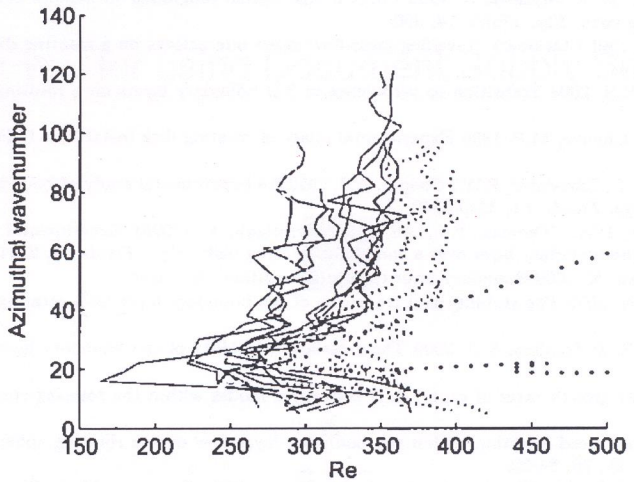

Figure 9: Neutral curves for smooth ($\cdots$), and rough (-) disks with a theoretical smooth curve (+)

roughnesses. Neutral stability curves taken from experimental data also show a decrease in the azimuthal wavenumber, but do not show the slight increase in R_{crit} predicted by the theory, only a decrease for all rough disks. Again, more curves need to be produced in the future for more roughnesses to confirm these results.

Acknowledgments

J. H. Harris would like to thank the Engineering and Physical Sciences Research Council for support, and both S. J. Garrett and P. J. Thomas for supervision and advice. Thanks also go to J. Chattaway for help with the experimental rig and to the technical staff at the University of Warwick for manufacturing the rough disks.

References

[1]Sirovich, L. & Karlson, S. 1997 Turbulent drag reduction by passive mechanisms, *Nature* **388**, 753.

[2]Carpenter, P.W. 1997 The right sort of roughness, *Nature* **388**, 713.

[3]Choi, K.-S., 2006 The rough with the smooth, *Nature* **440**, 754.

[4]Fransson, J.H.M., Talamelli, A., Brandt, L. & Cossu, C. 2006 Delaying transition to turbulence by a passive mechanism, *Phys. Rev. Lett.* **96**, 064501.

[5]Bechert, D.W. 2000 Experiments with three-dimensional riblets as and idealized model of shark skin, *Exp. Fluids* **28**, 403.

[6]Theodorsen & Regier 1945 Experiments on drag of revolving disks, cylinders and streamline rods at high speeds, National Advisory Committee for aeronautics, Report no. 793, Washington DC, USA.

[7]Smith, N.H. 1947 Exploratory investigation of laminar-boundary-layer oscillations on a rotating disk, National Advisory Committee for aeronautics, Technical Note no. 1227, Washington DC, USA.

[8]Gregory, N, Stuart, J.T. & Walker, W.S. 1955 On the stability of the three-dimensional boundary-layer with application to the flow due to a rotating disk, *Phil. Trans. Roy. Soc. A* **248**, 1955.

[9]Reed, H.L. & Saric, W.S. 1989 Stability of three-dimensional boundary layers *Annu. Rev. Fluid Mech.* **21**, 235.

[10]Saric, W.S., Reed, H.L. & White, E.B. 2003 Stability and transition of three-dimensional boundary layers, *Annu. Rev. Fluid Mech.* **35**, 413.

[11]Wimmer, M. 1988 Viscous flows and instabilities near rotating bodies, *Prog. Aerospace Sci.* **25**, 43.

[12]Owen, J.M. & Rogers, R.H. 1989 Flow and heat transfer in rotating-disc systems, vol. 1 - Rotor-stator systems (Research Studies, Taunton, Sommerset, U.K).

[13]Watanabe, T., Warui, H.M. & Fujisawa, N. 1993 Effect of distributed roughness on laminar-turbulent transition in the boundary layer over a rotating cone, *Exp. Fluids* **14**, 390.

[14]Corke, T.C. & Knasiak 1998 Stationary travelling cross-flow mode interactions on a rotating disk, *J. Fluid Mech.* **355**, 285.

[15]Corke, T.C. & Matlis, E.H. 2004 Transition to turbulence in 3-D boundary layers on a rotating disk - triad resonance, in[30]

[16]Jarre, S., Le Gal, P., & Chauve, M.P. 1996 Experimental study of rotating disk instability. II Forced flow, *Phys. Fluids* **11**, 2985.

[17]Colley, A.J., Thomas, P.J., Carpenter, P.W., Cooper, A.J. 1999 An experimental study of boundary-layer transition over a rotating, compliant disc, *Phys. Fluids.* **11**, 3340-3352.

[18]Colley, A.J., Carpenter, P.W., Thomas, P.J., Ali, R., Zoueshtiagh, F. (2006) Experimental verification of Type-II-eigenmode destabilization in the boundary layer over a compliant rotating disk, *Phys. Fluids* **18**, 054107.

[19]Schlichting, H. & Gersten, K. 2000 Boundary-layer theory (8th edition), Springer.

[20]Garrett, S.J. & Peake, N. 2002 The stability and transition of the boundary layer on a rotating sphere, *J. Fluid Mech.* **456**, 199-218.

[21]Garrett, S.J., Hussain, Z. & Stephen, S.O. 2009 The crossflow instability of the boundary layer on a rotating cone, *J. Fluid Mech.* **622**, 209-232.

[22]Garrett, S.J. 2010 Linear growth rates of type I & II convective modes within the rotating-cone boundary layer, *Fluid Dyn. Res.* **42**, 025504.

[23]Garrett, S.J. 2010 Vortex-speed selection within the boundary-layer flow over a rotating sphere placed in an enforced axial flow, *European J. Mech. B.*, **29**, 84-92.

[24]Miklavcic, M. & Wang, C.Y. 2004 The flow due to a rough rotating disk, *Z. angew. Math. Phys.* **55**, 235.

[25]Yoon, M. S., Hyun, J. M. & Park, J. S. 2007 Flow and heat transfer over a rotating disk with surface roughness, *International Journal of Heat and Fluid Flow* **28**, 262.

[26]Kármán, von Th. 1921 Ueber laminare und turbulente Reibung, *Z. Angew. Math. Mech.* **1**, 233.

[27]Banks, W. H. H. 1965 The boundary layer on a rotating sphere. *Q. J. Mech. Appl. Math* **18**, 443–454

[28]Lingwood, R.J. 1995 Absolute instability of the boundary layer on a rotating disk, *J. Fluid Mech.* **299**, 17.

[29]Malik, M. R. 1986 The neutral curve for stationary disturbances in rotating-disk flow. *J. Fluid Mech.* **164**, 275–287.

[30]Meier, G.E.A. & Sreenivasan, K.R. (Editors), 2004 Proceedings of the IUTAM Symposium on one hundred years of boundary layer research, Göttingen, Germany, August 12-14, Springer.

[31]Nikuradse, J. 1933 Stömungsgesetze in rauhen Rohren, *Forschg. Arb. Ing.-Wes.* No 361.